Research Article
doi.org/10.1002/chem.202200783

Molecular Magnetic Materials Based on $\{Co^{III}(Tp^*)(CN)_3\}^-$ Cyanidometallate: Combined Magnetic, Structural and ^{59}Co NMR Study

Siddhartha De,[a] Alexandrine Flambard,[a] Buqin Xu,[a] Lise-Marie Chamoreau,[a] Geoffrey Gontard,[a] Laurent Lisnard,[a] Yanling Li,[a] Marie-Laure Boillot,[b] and Rodrigue Lescouëzec*[a]

Abstract: The cyanidocobaltate of formula *fac*-$PPh_4[Co^{III}(^{Me2}Tp)(CN)_3]\cdot CH_3CN$ (**1**) has been used as a metalloligand to prepare polynuclear magnetic complexes (^{Me2}Tp = hydrotris(3,5-dimethylpyrazol-1-yl)borate). The association of **1** with in situ prepared $[Fe^{II}(bik)_2(MeCN)_2](OTf)_2$ (bik = bis(1-methylimidazol-2-yl)ketone) leads to a molecular square of formula $\{[Co^{III}\{(^{Me2}Tp)\}(CN)_3]_2[Fe^{II}(bik)_2]_2\}(OTf)_2\cdot 4MeCN\cdot 2H_2O$ (**2**), whereas the self-assembly of **1** with preformed cluster $[Co^{II}_2(OH_2)(piv)_4(Hpiv)_4]$ in MeCN leads to the two-dimensional network of formula $\{[Co^{II}_2(piv)_3]_2[Co^{III}(^{Me2}Tp)(CN)_3]_2\cdot 2CH_3CN\}_\infty$ (**3**). These compounds were structurally characterized via single crystal X-ray analysis and their spectroscopic (FTIR, UV-Vis and ^{59}Co NMR) properties and magnetic behaviours were also investigated. Bulk magnetic susceptibility measurements reveal that **1** is diamagnetic and **3** is paramagnetic throughout the explored temperature range, whereas **2** exhibits sharp spin transition centered at ca. 292 K. Compound **2** also exhibits photomagnetic effects at low temperature, selective light irradiations allowing to promote reversibly and repeatedly low-spin⇔high-spin conversion. Besides, the diamagnetic nature of the Co(III) building block allows us studying these compounds by means of ^{59}Co NMR spectroscopy. Herein, a ^{59}Co chemical shift has been used as a magnetic probe to corroborate experimental magnetic data obtained from bulk magnetic susceptibility measurements. An influence of the magnetic state of the neighbouring atoms is observed on the ^{59}Co NMR signals. Moreover, for the very first time, ^{59}Co NMR technique has been successfully introduced to investigate molecular materials with distinct magnetic properties.

Introduction

Cyanide coordination chemistry has been widely used for decades to yield polynuclear coordination clusters and extended networks with adjustable structural and physical features.[1] In particular, in the quest for building magnetic systems, the cyanide ligand has appeared advantageous because: (i) it can act as an efficient magnetic relay between paramagnetic spin carriers and thus promotes magnetic exchange interaction,[2] (ii) its ambidentate nature allows accessing to a variety of M–CN–M′ bimetallic systems, some of them showing valence tautomerism, and (iii) the linear nature of the cyanide bridge can provide directionality, which allows reliable prediction of the magnetic exchange interaction in the resulting compound by means of simple orbital-based model of the magnetic exchange interaction.[3] Moreover, a variety of cyanidometallates building blocks $[M(L)(CN)_x]^{n-}$ whose electronic properties and geometry can be modulated are achievable (L stands for a blocking ligand). This versatility makes possible the design of original molecular materials whose magnetic, optical, and electronic properties can be tuned in a systematic fashion through the self-assembly of preformed cyanido building blocks.[1d,3b–d] In our group, we have been particularly interested in the use of the *fac*-$[Fe^{III}(Tp)(CN)_3]^-$ complex (Tp = tris(pyrazol-1-yl)borate) that we first reported in 2002 and which we have used as a building block for designing molecular magnetic systems or redox active materials.[4] Over the years, other groups have successfully used this building-block and related Tp-based tris-cyanido complexes for designing original molecular magnetic materials such as Single Molecule Magnets (SMMs), Single Chain Magnets (SCMs), or stimuli-responsive systems.[4a,e,5] In particular the $[Fe^{III}(^{R}Tp)(CN)_3]^-$ complexes have been broadly used in the last decade to design switchable polynuclear complexes where temperature, pressure change or light irradiation can trigger a metal-metal charge transfer inside the $Fe^{II/III}$-CN-$M^{II/III}$ unit (M = Co, Mn).[5b,c,e,g,j,6] When

[a] Dr. S. De, Dr. A. Flambard, B. Xu, L.-M. Chamoreau, G. Gontard, Dr. L. Lisnard, Dr. Y. Li, Prof. R. Lescouëzec
Institut Parisien de Chimie Moléculaire, UMR CNRS 8232
Sorbonne Université, CNRS
75005 Paris (France)
E-mail: rodrigue.lescouezec@sorbonne-universite.fr

[b] Dr. M.-L. Boillot
Institut Chimie Moléculaire et Matériaux d'Orsay, UMR CNRS 8182
Université Paris-Saclay, CNRS
91405, Orsay (France)

Supporting information for this article is available on the WWW under https://doi.org/10.1002/chem.202200783

combined with $\{Fe^{II}(bik)_2(S)_2\}^{2+}$ or $\{Fe^{II}(Tp)(S)_3\}^{+}$ building blocks (bik = bis(1-methylimidazol-2-yl)ketone; S = labile solvent), we have also shown that tetra- or octa-metallic mixed valence spin-crossover (SCO) complexes can be obtained.[6a,7] In continuation of this work, we have recently reported the synthesis and structure of a diamagnetic analogue: the *fac*-$PPh_4[Co^{III}(^{Me2}Tp)(CN)_3]\cdot CH_3CN$ (**1**) building block featuring ^{Me2}Tp (hydrotris(3,5-dimethylpyrazol-1-yl)borate) ligand.[4c] As for its paramagnetic counterpart, this diamagnetic complex can also be used as a building-block to prepare polynuclear complexes with novel topology. Its diamagnetic nature does not prevent the observation of interesting magnetic properties as for example, its use as metalloligand toward $\{Fe^{II}(bik)_2(S)_3\}^{2+}$ units should lead to switchable systems. Actually, the main objective of this contribution is two-fold: (a) to explore the coordination chemistry of new cyanidometallate-derived molecular magnetic materials and (b) to investigate if ^{59}Co NMR -thanks to the NMR active nature of the Co(III) nuclei- can be used to probe the magnetic properties of these compounds. Actually, ^{59}Co is an NMR-active high sensitivity nucleus. It is a quadrupolar spin 7/2 nucleus with 100% natural abundance. ^{59}Co has also the broadest reported chemical-shift range, about 18 000 ppm, which stresses its sensitivity to the local structure.[8] So far, ^{59}Co solid-state NMR spectroscopy has been widely employed to probe various small molecules, battery materials, biological model systems, homogeneous catalysts and octahedral basic inorganic complexes.[9] In most cases, the cobalt ion exhibits a +III oxidation state (in some cases it is +I) and the complexes are diamagnetic.[10] When the cobalt atom carries unpaired electrons, the relaxation becomes too fast and no signal can be detected by standard NMR techniques. In our present work, we intend to probe the ^{59}Co NMR chemical shifts of the diamagnetic Co(III) ions belonging to the $\{Co^{III}(^{Me2}Tp)(CN)_3\}^{-}$ building block engaged in paramagnetic polymetallic species. As the cyanide is efficient in transmitting spin density, one can expect these signals to be sensitive to the magnetic state of the neighbouring metal ions. With these aims, we report here the use of the *fac*-$[Co^{III}(^{Me2}Tp)(CN)_3]^{-}$ as metalloligand: (a) toward the in situ formed mononuclear $[Fe^{II}(bik)_2(S)_2]^{2+}$ complex to obtain a molecular square complex exhibiting spin transition, (b) toward a preformed dinuclear $[Co^{II}_2(\mu\text{-}OH_2)(piv)_4(Hpiv)_4]$ complex (where Hpiv = pivalic acid or trimethylacetic acid) that results in a high nuclearity two-dimensional (2D) paramagnetic network. The ^{59}Co NMR chemical shift of these complexes and their temperature dependency are compared to the temperature dependent magnetic susceptibility (obtained from SQUID magnetometry) to probe the sensitivity of ^{59}Co chemical shift to the magnetic properties of the materials. The study of the SCO based compound is particularly suited for carrying out this study as the Fe(II) spin state can change from diamagnetic to paramagnetic upon increasing temperature.

Results and Discussion

Similarly to previously reported square complexes, the tetrametallic complex, $\{[Co^{III}(^{Me2}Tp)(CN)_3]_2[Fe^{II}(bik)_2]_2\}(OTf)_2\cdot 4MeCN\cdot 2H_2O$ (**2**) can be obtained by reacting **1** with the in situ prepared $[Fe^{II}(bik)_2(CH_3CN)_2](OTf)_2$ complex in acetonitrile at room temperature. **2** is isolated as dark red plate-like crystals after slow evaporation (yield: 66%). Compound **3**, $\{[Co^{II}_2(piv)_3]_2[Co^{III}(^{Me2}Tp)(CN)_3]_2\}_\infty$, is obtained by self-assembly of **1** with preformed dinuclear complex $[Co^{II}_2(\mu\text{-}OH_2)(piv)_4(Hpiv)_4]$ in CH_3CN.[11] It is isolated as purple prismatic crystals by slow evaporation of an acetonitrile solution (yield: 81%). It has already been observed that $[Co^{II}_2(\mu\text{-}OH_2)(piv)_4(Hpiv)_4]$ can recombine in solution to yield homo- and hetero-valent species with nuclearities ranging from three to fourteen Co ions.[11] This recombination is very much dependent on temperature, which has a strong influence on the nuclearity of the final compound. In the present case, we performed the reaction at room temperature, which maintains the dinuclear structure of the complex. The purity of all three complexes was determined by elemental analyses and thermal stability of these complexes was investigated by performing TGA (see Supporting Information).

Structure Analysis

$\{[Co(^{Me2}Tp)(CN)_3]_2[Fe(bik)_2]_2\}(OTf)_2\cdot 4MeCN\cdot 2H_2O$ (**2**) crystallizes as dark red plate-like crystals in the triclinic *P-1* space group. Its structure consists of $\{Co_2Fe_2\}$ square motifs, triflate anions, crystallisation water and acetonitrile molecules. In this centrosymmetric square complex the two $\{Co(^{Me2}Tp)(CN)_3\}^{-}$ building-blocks act as bis-monodentate ligands toward two *cis*-$\{Fe(bik)_2\}^{2+}$ units through two *cis* cyanide groups. The remaining terminal cyanide ligands adopt an anti-orientation relative to the $\{Fe_2(\mu\text{-}NC)_4Co_2\}$ skeleton (Figure 1). The crystal data obtained at 200 K show that the Co–CN–Fe edges are almost identical and their distance, ca. 4.972(4) Å, is typical for Co^{III}–CN–Fe^{II}_{LS} linkage (LS = low spin). The angles at each corner of the square slightly deviate from orthogonality [88.41(1)° and 90.60(1)° at Co1 and Fe1, respectively] and slightly distorted octahedral CoN3C3 and FeN6 surroundings result from the contribution of three nitrogen atoms of the tridentate $(^{Me2}Tp)^{-}$ ligand and three cyanide-carbon atoms [at Co] and four nitrogen atoms from two bidentate bik ligands plus two cyanide-nitrogen atoms [at Fe]. The distortions of the metal coordination sphere were analysed by continuous shape measurements using the SHAPE program.[12] The reported output (shape factor) allows assessing the matching between an idealized polyhedron and the actual coordination sphere: the lower the shape factor is, the better the matching between the actual coordination sphere and the idealized polyhedron. Here the lowest values calculated by SHAPE are obtained for the octahedron in both cases (0.059 for the Fe and 0.099 for the Co) and point to slightly distorted coordination spheres. The cyanide bridges are slightly bent on the Fe(II) side [Fe1–N1–C1 = 176.9(2)° and Fe1–N2–C2 = 173.9(2)°] and remain close to linearity on the Co(III) side [178.6(2)–179.3(2)°]. The Co^{III}–C_{cyano} bond lengths in the $[Co(^{Me2}Tp)(CN)_3]^{-}$ unit [values in the range 1.871(2)–1.873(2) Å] are in agreement with a low-spin cobalt(III). The Fe^{II}–N_{bik} [1.952(2)–1.982(2) Å] and Fe^{II}–$N_{cyanide}$

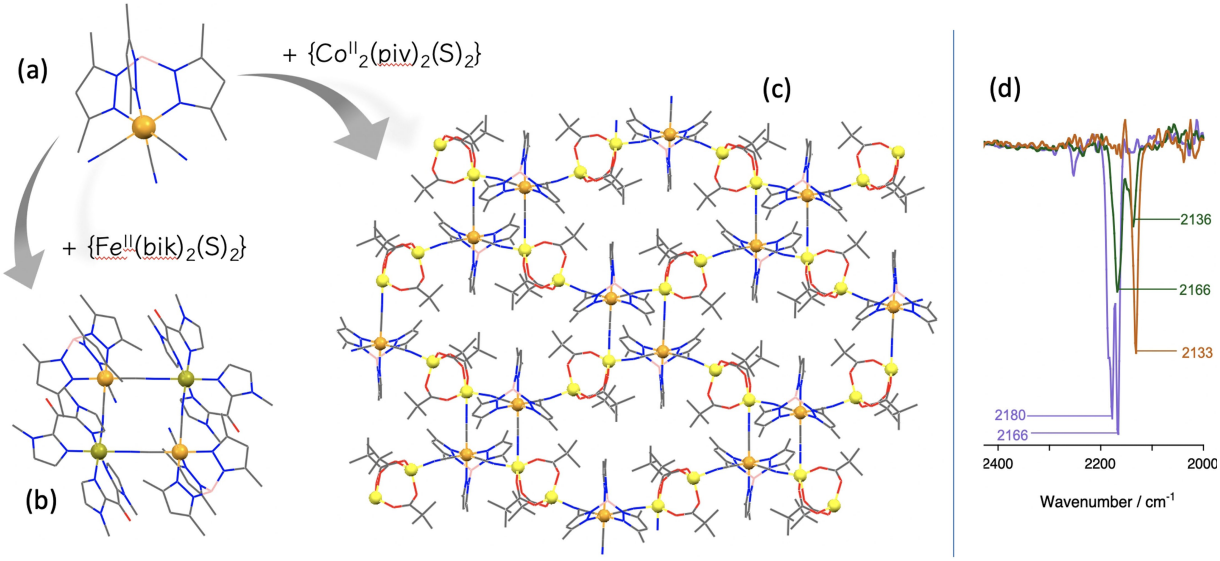

Figure 1. Perspective views of **(a)** the [Co^{III}(^{Me2}Tp)(CN)$_3$]$^-$ complex in **1**; **(b)** the {Co$^{III}_2$Fe$^{II}_2$}$^{2-}$ square complex in **2**; **(c)** the 2D network in **3**. Hydrogen atoms and solvent molecules are omitted for clarity. Light orange: Co^{III}, yellow : Co^{II}, light green : Fe^{II}. **(d)** Zoom of the FT-IR spectra of **1** (orange), **2** (green) and **3** (violet) showing the cyanide stretching vibrations.

distances [1.947(2) and 1.951(2) Å] at 200 K are coherent with the occurrence of a low-spin Fe(II) in a N_6 surrounding.[5c,6a,b,13] Indeed, these distances are comparable with those observed in previously reported cyanide-bridged tetra-nuclear {Fe$^{III}_2$Fe$^{II}_2$} and {Mo$^{V}_2$Fe$^{II}_2$} complexes containing a similar {Fe(bik$_2$)(NC)$_2$}$^{2+}$ entity.[6a,b] The spectroscopic and magnetic data also support the occurrence of a low-spin {Co$^{III}_{LS}$–CN–Fe$^{II}_{LS}$} pair below room temperature (see below). Furthermore, the molecular squares are connected to each other via hydrogen bonding between water molecule, terminal CN, and imidazolyl hydrogen atom (see Supporting Information). The shortest inter-square metal-metal bond distance is 9.317(1) Å. The terminal cyanide groups are connected to the triflate anions through two hydrogen-bonded water molecules along a CN(terminal)···O(water)···O-(OTf$^-$) path (see Supporting Information). The N_{CN}···O(water) and O(water)···O(OTf$^-$) contacts amount to 2.843(3) and 2.882(2) Å respectively, and the angle O(OTf$^-$)···O(water)···N($_{CN}$) is 128.64(8)°. Compound **3** crystallizes in a monoclinic $P2_1/c$ space group. Its structure consists of a neutral 2D network, which is made of [Co^{III}(^{Me2}Tp)(CN)$_3$]$^-$ complexes that are connected to three different [Co$^{II}_2$(piv)$_3$] units through three CN ligands (Figure 1). The 2D layer can be described as a network of hexa-nuclear {Co$^{III}_2$Co$^{II}_4$} motifs (see Figure 1 and Supporting Information) that are linked to each other by cyanide bridges (no oxidation state change is detected between the building block and the final material as described below). The {Co$^{III}_2$Co$^{II}_4$} motifs are made of two *fac*-[Co(^{Me2}Tp)(CN)$_3$]$^-$ units, each of which coordinates through *cis*-cyanide ligands to a Co(II) ion of the two [Co$^{II}_2$(piv)$_3$] bimetallic units in a square-like fashion. In the bimetallic unit, one of the Co(II) ions is tetra coordinated and the other is penta-coordinated. The SHAPE analysis performed on **3** reveals that the ideal structure of the Co(III) centre is close to an octahedron, whereas the penta-coordinated Co(II) centre exhibits a trigonal bipyramid (shape factor: 0.947) and the tetra-coordinated Co(II) centre has a distorted tetrahedral coordination sphere (shape factor: 1.229).[12] The penta-coordinated Co(II) centre coordinates to two nitrogen atoms from the CN bridges (forming the square motif) and three oxygen atoms belonging to three μ-κO:κO′ bridging pivalate (Me_3CCOO^-) groups, whereas the tetrahedral Co(II) centre coordinates to one nitrogen atom from the [Co(^{Me2}Tp)(CN)$_3$]$^-$ and three oxygen atoms from three μ-κO:κO′ bridging pivalate groups (see Supporting Information). In the {Co$^{III}_2$Co$^{II}_4$} core unit, the Co^{III}–CN–Co^{II} edges are quasi identical [4.962(1) and 5.040(1) Å] and the angles at the corners slightly deviate from orthogonality [Co^{III}–Co^{II}–Co^{III} = 91.39(1)° and Co^{II}–Co^{III}–Co^{II} = 88.61(1)°]. Although the cyanide bridges are bent on the Co(II) side [Co^{II}-N–C angles: 163.3(2) and 167.2(2)°], they remain close to linearity on the Co(III) side [Co^{III}–C–N angles: 172.4(2) and 179.5(2)°]. In the [Co-(^{Me2}Tp)(CN)$_3$]$^-$ subunit, the third cyanide ligand (Co^{III}–C3–N3) acts as a linker between neighbouring {Co$^{III}_2$Co$^{II}_4$} units. The Co^{III}–C_{cyano} bond distances range from 1.871(2) to 1.889(2) Å. These values are slightly higher than those observed in the related low-spin [Co(^{Me2}Tp)(CN)$_3$]$^-$ building block and coherent with a low-spin Co(III) ion. The angles subtended by the tripodal ligands at the Co(III) site slightly deviate from orthogonality [86.90(9) to 92.99(10)°]. Overall, X-ray analysis supports the presence of Co(III) and Co(II) ions at 200 K, and this observation is also coherent with the magnetic data (see below). The layers are quite well isolated from each other, the shortest intermolecular Co^{III}–Co^{III} and Co^{III}–Co^{II} distances between two layers being 9.033(1) and 10.055(1) Å, respectively. Relevant data regarding the Co(III) coordination spheres in these three complexes are given in Table 1. To sum up, the Co(III) centres in all these three compounds are low spin in nature and they hold an almost ideal octahedral geometry (shape factor S ≈ 0.1).

Table 1. Selected structural data and geometry of **1**, **2** and **3**. Distances in Å and angles in degrees.

	1	2	3
$d[Co^{III}(CN)_{bridging}]_{av}$	–	1.872(1)	1.872(2)
$d[Co^{III}\text{-}N(Tp)]_{av}$	1.993(6)	1.989(9)	1.975(7)
Σ for Co^{III} centre	11.5	13.7	14.0
Shape factor S (OC-6) for Co^{III} centre	0.119	0.099	0.099
Shortest intermolecular $Co^{III}\cdots Co^{III}$ distance	9.830(1)	9.779(1)	9.033(1)
$[(NC\text{-}Co^{III}\text{-}CN)_{bridging}]_{av}$ angle	–	88.23(7)	91(2)

FTIR Analysis

FTIR spectroscopy has been employed to characterize all three complexes and to get detailed information about the cyanide coordination mode involved in these complexes. Similarly to the cyanido-Fe(III) counterparts, the CN stretching vibration is also indicative of the redox state of the metal ion linked to the cyanide carbon atom, and of the bridging mode of the cyanide ligand.[14] The infrared spectrum of **1** obtained at room temperature exhibits characteristic B–H stretching vibration at 2531 cm^{-1} that is similar to that observed in the related Fe(III) building blocks. A unique cyanide stretching vibration is observed at 2131 cm^{-1}, close to that observed in $[Co(CN)_6]^{3-}$ (Figure 1d).[14a] This indicates that all cyanide ligands adopt a terminal coordination mode. The infrared spectrum of **2** exhibits B–H vibration around 2534 cm^{-1} and two cyanide vibrations are located at 2166 and 2136 cm^{-1} which are characteristic of bridging $[\{Co^{III}_{LS}(\mu\text{-}CN)Fe^{II}_{HS}\}]$ units (HS = high spin) and terminal cyanide ligands, respectively (Supporting Information).[14a,15] The infrared spectrum of **3** also displays strong B–H vibrations at 2553 and 2535 cm^{-1}. The stretching cyanide vibrations at 2180 and 2166 cm^{-1} are clearly shifted compared to **1**, and unambiguously indicate that all cyanide ligands adopt a bridging mode. The small stretching vibration around 2252 cm^{-1} can be ascribed to the CH_3CN molecules trapped in the crystal lattice.

Magnetic behaviour

Bulk molar magnetic susceptibility (χ_M) measurements were carried out on the fresh samples of **1**, **2** and **3**. The $\chi_M T$ *versus* T curves shown in Figure 2a reveal drastically different magnetic behaviours for the three compounds.

While compound **1** remains diamagnetic throughout the explored temperature range, as expected for a low-spin Co(III) complex ($S_{Co}=0$), compound **3** is paramagnetic in the same temperature range. In **3**, the $\chi_M T$ value for each $\{Co^{III}_2Co^{II}_4\}$ repeating unit of the 2D network amounts to 9.31 $cm^3\,mol^{-1}\,K$ at 300 K. This value lies within the expected range for the following set of magnetically isolated ions: two low-spin Co(III) ions ($S=0$), and four high-spin Co(II) ions ($S=3/2$). Two of them are tetrahedral ($2.1<\chi_M T<3.1\ cm^3\,mol^{-1}\,K$ per Co^{II} at 300 K) and the other two exhibit a trigonal bipyramidal geometry ($2.4<\chi_M T<3.4\ cm^3\,mol^{-1}\,K$ per Co^{II} at 300 K).[16] Upon lowering the temperature, the $\chi_M T$ value remains almost unchanged down to 45 K, which support the absence of significant magnetic

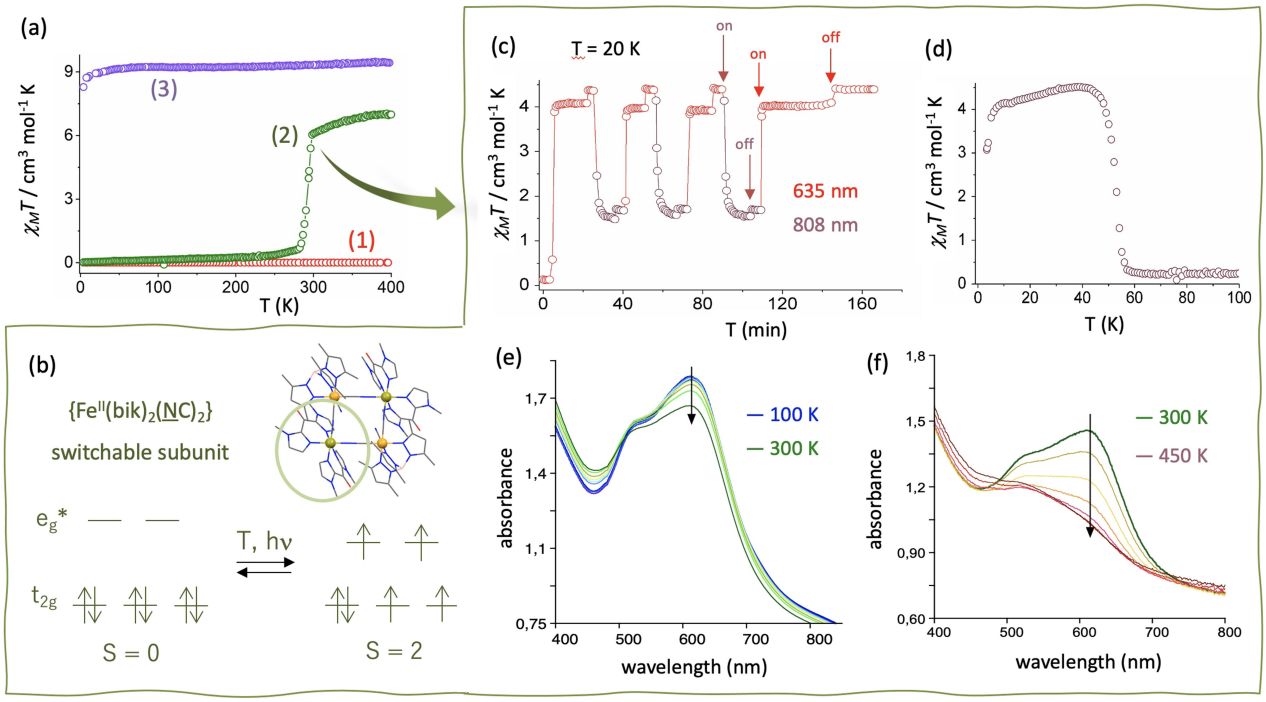

Figure 2. (a) $\chi_M T$ *versus* T curves of **1**–**3. (b)** scheme of the electronic configuration change occurring in the $\{Fe^{II}(bik)_2(NC)_2\}$ SCO subunit in compound **2**. **(c)** $\chi_M T$ *versus* irradiation time at 635 and 808 nm in **2**. Red and grey arrows indicate when the 635 and 808 lights are switched on and off. The small jump after switching off the light are due to the thermalization. **(d)** $\chi_M T$ *versus* T curve of the photoinduced paramagnetic state ($\lambda_{exc}=635$ nm) upon heating in darkness in **2**. **(e–f)** Solid-state UV-vis spectra of **2** upon heating between 100 and 300 K (e) and 300–450 K (f).

interaction between the ions. Below this temperature, a slight decrease down to $\chi_M T = 8.13\ cm^3\,mol^{-1}\,K$ at 2 K is observed. This decrease is probably associated to weak antiferromagnetic exchange interactions between high-spin Co^{II} sites in **3** or to the effect of magnetic anisotropy (Figure 2a). In contrast, **2** shows a strong temperature dependence of its $\chi_M T$ product (Figure 2a): the $\chi_M T$ curve of a fresh sample of **2** exhibits a plateau up to ca. 270 K with a $\chi_M T$ value close to zero and then sharply increases around room temperature to reach a pseudo plateau, as the $\chi_M T$ value increases smoothly from 6.01 $cm^3\,mol^{-1}\,K$ at 298 K to 7.02 $cm^3\,mol^{-1}\,K$ at *ca.* 358 K. This behaviour is ascribed to a spin-state change of the two $\{Fe^{II}(bik)_2(\underline{N}C)_2\}$ subunits with a transition temperature of $T_{1/2} = 292$ K. The non-zero $\chi_M T$ value measured at low temperature (ca. 0.34 $cm^3\,mol^{-1}\,K$) is twice that of the value measured for the Co(III) monometallic precursor and it is likely due to the temperature independent paramagnetism. The overall variation of the $\chi_M T$ value is close to that expected for a spin-crossover from the low-spin $(t_{2g})^6$ electronic configuration to the high spin $(t_{2g})^4(e_g)^2$ one ($\Delta\chi_M T = 7.26\ cm^3\,mol^{-1}\,K$ with $g \approx 2.2$).[5c,6a–c,17] The net increase of ca. 6.68 $cm^3\,mol^{-1}\,K$ corresponds to an almost complete spin-crossover of the two Fe(II) ions (ca. 92% of LS – HS conversion). This represents a larger spin-state conversion than the one previously reported in the related tetrametallic $\{[Mo^{V}(CN)_8]_2[Fe^{II}(bik)_2]_2\}^{2-}$ cyanido-bridged complex ($T_{1/2} \sim 350$ K) containing the same $\{Fe^{II}(bik)_2(\underline{N}C)_2\}$ SCO subunit. However, it compares well with those reported in the analogous mixed-valence $\{[Fe^{III}(Tp)(CN)_3]_2[Fe^{II}(bik)_2]_2\}^{2+}$ and $\{[Fe^{III}(^{Me2}Tp)(CN)_3]_2[Fe^{II}(bik)_2]_2\}^{2+}$ square complexes.[6a,b,7a] The sharp spin-transition in **2** is strongly affected by heating. Indeed, the transition becomes gradual after heating at 400 K and is shifted toward lower temperature (see Supporting Information). This can be associated to the loss of crystallization solvent molecules, which occurs inside the magnetometer in the high temperature range. The shift of $T_{1/2}$ toward lower temperature upon desolvation was already observed in the $\{Fe^{III}_2Fe^{II}_2\}$ and $\{Mo^{V}_2Fe^{II}_2\}$ square complexes mentioned above (table 2).[6a] As previously suggested in another study, one could assume that the removal of the crystallization solvent molecules, would release the steric constraints imposed by the crystal lattice so that the complex would easily enters the HS state.[18] Finally it is worth noticing that the transition temperature measured on the desolvated sample ($T_{1/2} = 213$ K) is close to the value observed in the related $\{Fe^{III}_2Fe^{II}_2\}$ square complex where $[Fe^{III}(^{Me2}Tp)(CN)_3]$ acts as metalloligand (223 K).[7a] In contrast, the square complexes based on the non-methylated metalloligand $[Fe^{III}(Tp)(CN)_3]$ showed spin-transition well above 400 K. This comparison suggests that both $[Fe^{III}(^{Me2}Tp)(CN)_3]^-$ and $[Co^{III}(^{Me2}Tp)(CN)_3]^-$ metalloligands are weaker N-donating ligands than the $[Fe^{III}(Tp)(CN)_3]^-$ complex.[7a]

Table 2. Selected data on switchable properties of SCO complexes containing $\{Fe^{II}(bik)_2(N\text{-})_2\}$ unit. Data in parentheses relate to desolvated phases. Ø indicate no LIESST effect.

	$T_{1/2}$ [K]	T_{LIESST} [K]	most efficient wavelength (nm)	Ref.
$[Fe(bik)_3](BF_4)_2$	316	ca 50	635	[21]
$[Fe(bik)_2(NCS)_2]$	260	<20	900	[19]
$[Fe(bik)_2(NCSe)_2]$	326	<20	900	[19]
$\{[Fe(Tp)(CN)_3]_2[Fe(bik)_2]_2\}$ $[Fe(Tp)(CN)_3]_2\cdot 18H_2O,4CH_3OH$	330 (240)	Ø (ca 45)	Ø (750)	[6a]
$\{[Fe(^{Me2}Tp)(CN)_3]_2[Fe(bik)_2]\}_2$ $(ClO_4)_2\cdot 2H_2O$	223	35	635 and 900	[7a]
$\{[Fe(Tp)(CN)_3]_2[Fe(bik)_2]\}_2$ $(ClO_4)_2\cdot 2CH_3CN$	>400	Ø	Ø	[7a]
$\{[Fe(Tp)(CN)_3]_2[Fe(bik)_2]\}_2$ $(BF_4)_2\cdot 2CH_3OH$	>400	<20	808[a]	[7a]
$\{[Co(^{Me2}Tp)(CN)_3]_2[Fe(bik)_2]\}_2$ $(OTf)_2\cdot 4MeCN\cdot 2H_2O$ (2)	ca 292	ca 55	405, 532, 635 or 900	This work
$\{[Mo(CN)_8]_2[Fe(bik)_2]_2\}$ $(HMeIm)_2\cdot 5H_2O,CH_3CN$	ca 350 (300)	ca 48	405	[6b]
$(HNBu_3)_2\{[W_2(CN)_8]_2[Fe(bik)_2]_2\}$ $\cdot 6H_2O\cdot CH_3OH$	ca 370 (305)	Ø (ca 63)	Ø (532)	[22]

[a] only 808, 405 and 532 nm wavelengths were tested in that case.

Photomagnetic behaviour and thermochromism in 2

The switchable properties of **2** were investigated in more depth and reveal both photomagnetic and thermochromic effects beside the thermally-induced spin transition observed in magnetometry (Figure 2b-f). In fact, the magnetization of **2** strongly increases when exposed to light irradiation at low temperature (20 K). Note that these measurements were done on fresh samples of **2** and no photomagnetic effects were observed on the desolvated sample. Different laser-diodes were tested, $\lambda = 900$, 808, 635, 532 and 405 nm (with the respective powers: ca. 5, 11, 11, 12 and 5 $mW\,cm^{-2}$), all of them inducing a rapid increase of the $\chi_M T$ value upon irradiation (see Supporting Information). Such photomagnetic effect in Fe(II) SCO complex is ascribed to a Light-Induced Excited Spin-State Trapping (LIESST) effect, the low-spin Fe(II) ($S = 0$) state being converted into a metastable high-spin Fe(II) ($S = 2$) through the photo-induced population of transient excited state(s). The maximum conversion is observed at 635 nm, where the $\chi_M T$ value increases from ca. 0.21 to 4.51 $cm^3\,mol^{-1}\,K$. This increase corresponds approximately 66% of the thermally induced LS-HS conversion. All other wavelengths lead to slightly lower conversion rate, except that at 808 nm, which leads to a much lower value of 1.6 $cm^3\,mol^{-1}\,K$ (*ca* 21% of the thermally-induced conversion). The distinct efficiency of the 635 and 808 nm wavelengths in promoting LIESST effect could be related to different photoconversion pathways,[19] or to a "reverse-LIESST" effect.[20] Actually, the irradiation at 808 nm of the photoinduced metastable state obtained at 635 nm induces a decrease of the $\chi_M T$ value down to ca. 1.6 $cm^3\,mol^{-1}$ (see Figure 2c). This demonstrates that the 808 nm wavelength is also efficient in promoting a partial back-conversion from the metastable HS state to the diamagnetic LS state. The photo-stationary state ($\chi_M T \sim 1.6\ cm^3\,mol^{-1}\,K$) obtained when irradiating at 808 nm thus represents the equilibrium state between the LS→HS and the HS→LS photoconversion. Interestingly, the magnetisation can thus be modulated by successive light irradiation, demonstrating that the system can be repeatedly switched on and off by selective irradiations at 625 and 808 nm. Finally, the thermal

stability of the photo-induced metastable state was then probed by measuring the $\chi_M T$ versus T upon heating (at 0.4 K/min) after irradiation at 635 nm. The light-induced metastable paramagnetic state persists up to ca. $T_{LIESST} = 55$ K (determined as the inflexion point of the $\chi_M T$ versus T curve) in the present experimental conditions (Figure 2d). Note that the change of $\chi_M T$ value below ca. 10 K can be ascribed to the zero-field splitting effect of the pseudo-octahedral Fe(II) high-spin metastable state. In compound **2** the T_{LIESST} temperature (determined as the inflexion point of the $\chi_M T$ relaxation curve) is somehow higher than that measured under the exact same experimental conditions in the related tetrametallic $\{[Fe^{III}(^{Me2}Tp)(CN)_3]_2[Fe^{II}(bik)_2]_2\}^{2+}$ ($T_{LIESST} = 35$ K) $\{[Fe^{III}(Tp)(CN)_3]_2[Fe^{II}(bik)_2]_2\}^{2+}$ ($T_{LIESST} = 45$ K) and $\{[Mo^{V}(CN)_8]_2[Fe^{II}(bik)_2]_2\}^{2-}$ ($T_{LIESST} = 48$ K) complexes, which all contain the $\{Fe^{II}(bik)_2(NC–)_2\}$ subunits.[5c,6a,7a] It is worth noticing that the excitation wavelength allowing the highest LIESST effect in the $\{Fe^{II}(bik)_2(NC–)_2\}$ subunits clearly depends on the nature of the cyanido-metalloligand as shown in table 2.[5c,6a,b,7a]

Compound **2** also shows a significant thermochromic effect associated to the thermally-induced spin-state change. Indeed, the UV-vis spectrum of **2** recorded at low temperature (*ca* 100 K) exhibits a strong band centred at 612 nm. This band can be ascribed to the metal to ligand charge transfer (MLCT) band of the $\{Fe^{II}(bik)_2(NC–)_2\}$ chromophores (Figure 2e and Figure 2f) as already observed in the previously reported molecular $\{Fe^{III}_2Fe^{II}_2\}$ and $\{Mo^{V}_2Fe^{II}_2\}$ square complexes containing the same $\{Fe^{II}(bik)_2(NC–)_2\}$ subunit.[6a,b,7a] The intensity of the band notably decreases upon heating, which is coherent with a spin transition as observed in the related square complexes.[5c,6a,b,7a] More specifically, the intensity decrease is due to the larger metal-ligand bond length in the high-spin state, which results in a smaller overlap between metal-centred and ligand-centred orbitals as compared to the low-spin state.[20] It is worth noticing that the change in the optical properties cover a broader temperature range than the one measured in SQUID magnetometry. This is related to the different experimental conditions used for both measurements (see Supporting Information).

Solid-state ^{59}Co NMR analysis

In previous works, we showed that NMR active nuclei of diamagnetic ions such as ^{113}Cd could be used as local probe to access accurate information on the local structure and electronic states of paramagnetic cyanide-based compounds.[23] For example, we showed that ^{113}Cd NMR was efficient in revealing the electronic state changes occurring upon reversible Li^+ intercalation in nanoporous CdFe Prussian blue analogues (PBAs).[23c] This information is made accessible in a M–CN–Cd pair as the changes of electronic/magnetic state on the M ion can be felt by the diamagnetic NMR active Cd(II) ion. In a similar manner, the present study offers the opportunity of investigating the efficiency of ^{59}Co NMR in sensing the magnetic state of cyanide-based complexes containing the Co–CN–M linkage, where M is the paramagnetic source and the low-spin Co(III) located on the C cyanide atom acts as the NMR probe. The situation is more challenging as the ^{59}Co nucleus bears a 7/2 nuclear spin with a rather large quadrupole moment that can lead to very broad NMR features in the solid-state (whose signal width increase with the asymmetry of the environment). However, the ^{59}Co nucleus has a 100% abundancy and its receptivity is about 1500 times better than that of ^{13}C. Moreover, among all NMR active nuclei, the ^{59}Co nucleus exhibits the broadest chemical shift range, of ca. 18000 ppm (−4000 to 14000 ppm). This has been attributed to the occurrence of an important contribution from the temperature independent paramagnetism ("TIP") that is related to the 3d nature of the Co atom.[24] Briefly, the TIP contribution to the experimental chemical shift, δ^{TIP}, which is to be added to the usual diamagnetic contribution to the chemical shift, $\delta^{exp} = \delta^{dia} + \delta^{TIP}$, arises from the mixing of the $t_{2g}{}^6$ ground state and the excited electronic states (such as the $(t_{2g})^5(e_g)^1$ configuration). The mixing is inversely related to the energy difference between these states and it is thus sensitive to the ligand field and the nature of the ligand in the coordination sphere.[25] Besides the TIP contribution, the experimental chemical shift bears in the case of **2** and **3** a paramagnetic contribution that arises from the hyperfine interaction of the ^{59}Co nuclear spin with the neighbouring paramagnetic sources. The hyperfine interaction can be decomposed into a through-space dipolar contribution (δ^{dip}) and a through-bond contact contribution (δ^{con}).[26] This last term is due to the delocalization of the spin density from the neighbouring paramagnetic centres to the probed nucleus through the cyanide bridge. In our previous study on CdFe PBA materials, we observed that the dipolar contribution remained moderate in comparison to the contact term. A simple calculation based on a point dipole model (see Supporting Information) would lead to dipolar contribution of ca. 5–30 ppm in the case of a Co^{III}_{dia}–CN–Co^{II} pair (depending on the orientation of the magnetic axis). In summary, in **2** and **3** the experimental chemical shift sums up the four contributions: $\delta^{exp} = \delta^{dia} + \delta^{TIP} + \delta^{con} + \delta^{dip}$

As the first coordination sphere of the Co^{III} ions are identical in all three compounds, which exhibit the same *fac*-$[Co(^{Me2}Tp)(CN)_3]^-$ units (see structural data), one can assume that the TIP contributions are similar in **1**–**3**. This assumption seems to be confirmed by the magnetic measurements. In fact, at low temperatures, the non-zero $\chi_M T$ values of the compounds **1** and **2** are similar (*ca* 0.17 $cm^3 mol^{-1}$ K per Co units) and can be ascribed to similar TIP contributions as these fresh materials are in a diamagnetic ground state (the TIP contribution cannot be estimated in **3** because the $\chi_M T$ value at low temperature is dominated by the paramagnetic contribution). In first approximation, compound **1** can thus be used as a reference for estimating the diamagnetic and TIP contribution $\delta^{dia} + \delta^{TIP}$ that are present in **2** and **3**. By subtracting the experimental shift of **1** to that of **2** and **3**, one can thus estimate the hyperfine contribution in **2** and **3**, $\delta^{con} + \delta^{dip}$, that is related to their paramagnetic nature.

^{59}Co NMR spectra of powder samples of **1**–**3** were recorded at 16.4 T in static echo conditions (Figure 3) and under Magic Angle Spinning (MAS) conditions for **1** (see Supporting

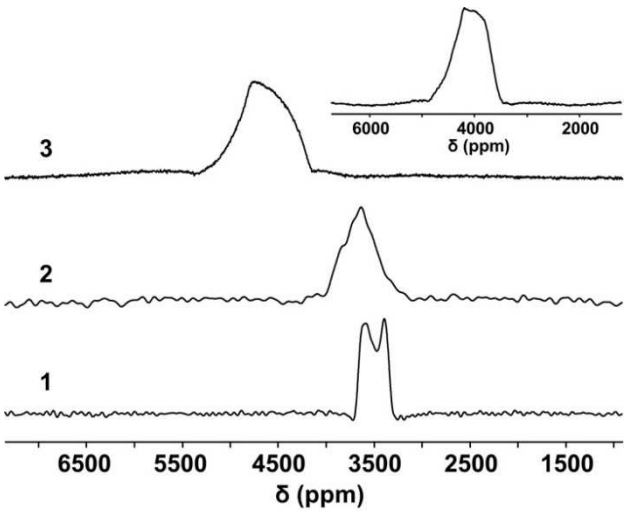

Figure 3. ^{59}Co NMR experimental spectra of stationary samples (fresh) of **1**, **2** and **3** acquired at 21.10 T, 260 K. Inset represents static NMR spectra of a previously desolvated (in TGA) sample of **2** at 260 K.

Information). The NMR line shapes in **1**–**3** suffer from an expected quadrupolar broadening. Only the compound **1** has been simulated and estimates of the quadrupolar coupling parameters were obtained.[10b,d] Note that these simulations cannot be carried out for **2** and **3**. To our knowledge, there is at the moment no software that can extract the different diamagnetic and paramagnetic contributions from solid-state ^{59}Co spectra.

The ^{59}Co isotropic chemical shifts (δ_{iso}) is thus only accessible for the diamagnetic compound **1**: $\delta_{iso} = +3590$ ppm (see Supporting Information). The comparison of δ_{iso} with the gravity center of this ^{59}Co signal, $\delta_G = 3495$ ppm allows estimating the shift induced by the quadrupolar coupling, $\delta_{QIS} = -95$ ppm. For **2** and **3**, we only access the δ_G which is expected to be close to the isotropic shift. For **2** at 260 K $\delta_G =$ 3593 ppm, while for **3** $\delta_G = 4754$ ppm (260 K). The chemical shift of the ^{59}Co nucleus for **3** is thus significantly shifted compared to that of the diamagnetic reference **1**. Its hyperfine contribution that arises from the presence of the neighbouring Co(II) ions is of the order of 1250 ppm. In contrast, **2** shows a smaller hyperfine positive shift of approx. +100 ppm when compared to **1**. It could come from the occurrence of a small fraction of neighbouring high-spin Fe(II) ions (as shown in the magnetic measurement in Figure 2), but such a small shift can also be ascribed to the differences observed in the second coordination sphere of the Co(III) ions in **1** and **2**. Indeed, the coordination of Fe(II) Lewis acid to the nitrogen cyanide of the $\{Co(^{Me2}Tp)(CN)_3\}$ units in **2** decreases the electron density onto the cyanide ligand and should reduce the ligand field on the Co(III) ion. This can lead to a positive shift of the ^{59}Co chemical shift as generally observed in Co(III) octahedral complexes.[24b] In contrast with our previous ^{113}Cd NMR studies on paramagnetic cyanide-based complexes where strongly shifted NMR signals were observed, here the measured ^{59}Co chemical shifts remain in the usual diamagnetic range for cyanido Co(III) complexes. Actually, the ^{59}Co chemical shift of cyanido complexes varies from 0 ppm for the $K_3[Co^{III}(CN)_6]$ with very strong ligand field (ca. 38000 cm^{-1}) to 6700 ppm for the $[Co^{III}(NH_3)_5(CN)]Cl_2$ complex that contains only one cyanide group.[9a] The *fac*-$[Co^{III}(NH_3)_3(CN)_3]$ complex that is closely related to **1** shows a similar chemical shift of 3315 ppm.[27] In order to clarify if the displacements in the chemical shifts are due to the hyperfine contribution or to ligand field effects, we have investigated the temperature dependence of the chemical shift. In **3**, the chemical shift value decreases of ca. 150 ppm upon heating the sample from 260 to 320 K (details in Supporting Information). This observation is in line with the paramagnetic nature of the compound. Indeed, according to the Curie law, the magnetization of a paramagnetic complex is inversely proportional to the temperature. Chemical shift should thus roughly follow the same trend with temperature as chemical shift can be visualised as local magnetic susceptibility.[28] Hyperfine contribution seems therefore to be responsible for the chemical shift in **3**. In contrast compound **2** shows a noticeable increase of the ^{59}Co chemical shift value of ca. +440 ppm from 260 to 320 K (table S3). This shift is well beyond the usual increase that is generally observed in diamagnetic Co(III) complexes, and which is ascribed to the lengthening of the Co-Ligand distance upon temperature increase and weakening of the ligand field (ca. +1.4 ppm/K for the $K_3[Co(CN)_6]$]).[28] Here, the strong positive shift is to be ascribed to the thermally-induced spin-transition occurring on the neighbouring Fe(II) ions upon heating. As the local magnetic susceptibility of the compound increases with temperature, the chemical shift value also increases.

At this stage, two points are worth commenting when comparing the present results on Co^{III}–CN–M^{II} systems with the previous one on Fe^{III}–CN–Cd^{II} systems. In contrast with the previous ^{113}Cd NMR studies, the NMR ^{59}Co chemical shifts are relatively small and remain in the diamagnetic range, indicating that only a small amount of spin density is transferred from the Fe^{II}/Co^{II} paramagnetic source to the Co(III) ion through the cyanide bridge. Their positive sign also contrasts with the negative sign observed for the ^{113}Cd in Fe^{III}–CN–Cd^{II} pairs. This also hints to a smaller amount of spin density transferred from the paramagnetic source to the NMR active nucleus in the Co^{III}–CN–M^{II} linkage than in Fe^{III}–CN–Cd^{II} one. This may be related to the nature of the Fe^{III}–CN and the CN–Fe^{II}/Co^{II} bonds. The spin density delocalization from the paramagnetic Fe(III) centre to the Cd ion through the CN ligand was shown to be efficient as the CN ligand acts as both σ-donor and π-acceptor ligand when coordinated via its carbon atom. This ensures efficient delocalization of the spin density from the paramagnetic ion into the π-orbital of both C and N atoms.[29] Then, polarization mechanism leads to negative spin density onto the Cd ion.[23a] In contrast, the N donor atom is involved in σ-donation with the paramagnetic metal ion in Co^{III}–CN–M^{II}. The delocalization of spin density from the Co(II) in **3** to the CN bridge may thus be weaker and mainly involve the N atom. A polarization mechanism through the Co^{II}–N–C pathway should then lead to negative and positive spin density onto the C and Co^{III} centers, respectively.

Conclusions

The Co(III) tricyanido building block, $[Co(^{Me2}Tp)(CN)_3]^-$, was used as metalloligand for the generation of a switchable molecular $\{Co^{III}_2Fe^{II}_2\}$ square (**2**) and high nuclearity 2D $\{Co^{III}_2Co^{II}_4\}_n$ network (**3**). The $\{Co^{III}_2Fe^{II}_2\}$ square complex behaves as a molecular switch: a thermally induced cooperative spin transition occurs on the Fe^{II} sites near room temperature. This induces drastic changes both in the magnetic state of the material and in its optical properties. In particular, strong changes are observed in the intensity of the charge transfer bands located in the visible region. The cooperative nature of the spin transition is lost upon heating the material above room temperature, likely because of the loss of intermolecular interaction associated with the removal of solvent crystallization molecules. A photomagnetic effect ("LIESST effect") is also observed at low temperature. The photoconversion is efficient in a broad energy range that corresponds to the MLCT band but also at 900 nm as observed in related complexes. Interestingly, a reverse-LIESST effect is observed at 808 nm, which permits to reversibly and repeatedly control the magnetic state of the system by selective irradiation. In contrast, the two-dimensional $\{Co^{III}_2Co^{II}_4\}_n$ compound remains paramagnetic throughout the explored temperature range and shows a Curie-like magnetic behaviour in a broad temperature range that accounts for very weak magnetic exchange coupling between the Co^{II} paramagnetic sources. The three compounds – the diamagnetic precursor (**1**), the molecular switch (**2**) and the paramagnetic network (**3**) – were used as model systems to investigate the use of ^{59}Co NMR as a probe for analysing the electronic and magnetic states of cyanido-based materials. The ^{59}Co NMR study at variable temperature showed that the chemical shifts are clearly correlated to the magnetic state of the material: "the more paramagnetic, the more shifted". This allows the indirect detection of the spin-state change occurring on the neighbouring Fe(II) SCO centre in the Co^{III}–NC–Fe^{II} linkage. To our knowledge this study represents the first report of solid state ^{59}Co NMR spectroscopic characterization of a spin-crossover compound. Interesting differences of sign and intensity are also observed in the paramagnetic chemical shifts of the Co and Cd diamagnetic probes in the M→C–N→Cd and M→N–C→Co linkages, where M is a paramagnetic source. These differences hint that a smaller spin density is transferred in the second case. This is likely related to the different bonding scheme between the paramagnetic source and the cyanide ligand depending on the nature of the donor atom C/N. Further experimental ^{13}C and ^{15}N NMR studies and theoretical calculation are now necessary to deepen our knowledge on the differences in spin density extension mechanisms.

CCDC2117924 (2) and 2117925 (3) contain the supplementary crystallographic data for this paper. These data are provided free of charge by The Cambridge Crystallographic Data Centre

Acknowledgements

The authors acknowledge the Centre National de la Recherche Scientifique, Sorbonne Université, Université Paris-Saclay for their financial support.

Conflict of Interest

The authors declare no conflict of interest.

Data Availability Statement

The data that support the findings of this study are available from the corresponding author upon reasonable request.

Keywords: magnetic properties · spin transition · cobalt · cyanides · NMR spectroscopy

[1] a) M. Shatruk, C. Avendano, K. R. Dunbar in *Cyanide-Bridged Complexes of Transition Metals: A Molecular Magnetism Perspective*, John Wiley & Sons, Ltd, **2009**, pp. 155–334; b) W. R. Entley, G. S. Girolami, *Science* **1995**, *268*, 397–400; c) A. Ludi, H. U. Güdel, In *Inorganic Chemistry. Structure and Bonding*, vol 14. Springer, Berlin, Heidelberg, **1973**, pp. 1–21; d) M. Verdaguer, A. Bleuzen, V. Marvaud, J. Vaissermann, M. Seuleiman, C. Desplanches, A. Scuiller, C. Train, R. Garde, G. Gelly, C. Lomenech, I. Rosenman, P. Veillet, C. Cartier, F. Villain, *Coord. Chem. Rev.* **1999**, *190–192*, 1023–1047; e) D. F. Shriver, In *Structure and Bonding*, vol. 1, Springer, Berlin, Heidelberg, **1966**, pp. 32–58.

[2] J. Cano, E. Ruiz, S. Alvarez, M. Verdaguer, *Comments on Inorg. Chem.* **1998**, *20*, 27–56.

[3] a) A. Dei, *Inorg. Chim. Acta* **1992**, *191*, 279; b) E. Dujardin, S. Ferlay, X. Phan, C. Desplanches, C. Cartier dit Moulin, P. Sainctavit, F. Baudelet, E. Dartyge, P. Veillet, M. Verdaguer, *J. Am. Chem. Soc.* **1998**, *120*, 11347–11352; c) S. Ferlay, T. Mallah, R. Ouahès, P. Veillet, M. Verdaguer, *Nature* **1995**, *378*, 701–703; d) Ø. Hatlevik, W. E. Buschmann, J. Zhang, J. L. Manson, J. S. Miller, *Adv. Mater.* **1999**, *11*, 914–918; e) S. M. Holmes, G. S. Girolami, *J. Am. Chem. Soc.* **1999**, *121*, 5593–5594.

[4] a) R. Lescouëzec, J. Vaissermann, F. Lloret, M. Julve, M. Verdaguer, *Inorg. Chem.* **2002**, *41*, 5943–5945; b) K. Ridier, A. Mondal, C. Boilleau, O. Cador, B. Gillon, G. Chaboussant, B. Le Guennic, K. Costuas, R. Lescouëzec, *Angew. Chem. Int. Ed.* **2016**, *55*, 3963–3967; *Angew. Chem.* **2016**, *128*, 4031–4035; c) S. De, A. Flambard, D. Garnier, P. Herson, F. H. Köhler, A. Mondal, K. Costuas, B. Gillon, R. Lescouëzec, B. Le Guennic, F. Gendron, *Chem. Eur. J.* **2019**, *25*, 12120–12136; d) J.-R. Jiménez, A. Sugahara, M. Okubo, A. Yamada, L.-M. Chamoreau, L. Lisnard, R. Lescouëzec, *Chem. Commun.* **2018**, *54*, 5189–5192; e) D. Li, S. Parkin, G. Wang, G. T. Yee, S. M. Holmes, *Inorg. Chem.* **2006**, *45*, 1951–1959; f) M.-X. Yao, Q. Zheng, X.-M. Cai, Y.-Z. Li, Y. Song, J.-L. Zuo, *Inorg. Chem.* **2012**, *51*, 2140–2149.

[5] a) R. Lescouëzec, J. Vaissermann, C. Ruiz-Pérez, F. Lloret, R. Carrasco, M. Julve, M. Verdaguer, Y. Dromzee, D. Gatteschi, W. Wernsdorfer, *Angew. Chem. Int. Ed.* **2003**, *42*, 1483–1486; *Angew. Chem.* **2003**, *115*, 1521–1524; b) J. Mercurol, Y. Li, E. Pardo, O. Risset, M. Seuleiman, H. Rousselière, R. Lescouëzec, M. Julve, *Chem. Commun.* **2010**, *46*, 8995–8997; c) A. Mondal, Y. Li, M. Seuleiman, M. Julve, L. Toupet, M. Buron-Le Cointe, R. Lescouëzec, *J. Am. Chem. Soc.* **2013**, *135*, 1653–1656; d) L. M. Toma, R. Lescouëzec, F. Lloret, M. Julve, J. Vaissermann, M. Verdaguer, *Chem. Commun.* **2003**, 1850–1851; e) D. Siretanu, D. Li, L. Buisson, D. M. Bassani, S. M. Holmes, C. Mathonière, R. Clérac, *Chem. Eur. J.* **2011**, *17*, 11704–11708; f) D. Li, S. Parkin, G. Wang, G. T. Yee, A. V. Prosvirin, S. M. Holmes, *Inorg. Chem.* **2005**, *44*, 4903–4905; g) M. Nihei, Y. Sekine, N. Suganami, K. Nakazawa, A. Nakao, H. Nakao, Y. Murakami, H. Oshio, *J. Am. Chem. Soc.* **2011**, *133*, 3592–3600; h) S. Wang, J.-L. Zuo, S. Gao, Y. Song, H.-C. Zhou, Y.-Z. Zhang, X.-Z. You, *J. Am. Chem. Soc.* **2004**, *126*, 8900–8901; i) S. Wang, J.-L. Zuo, H.-C. Zhou, H. J. Choi, Y. Ke, J. R. Long, X.-Z. You, *Angew. Chem. Int. Ed.* **2004**, *43*, 5940–5943; *Angew. Chem.* **2004**, *116*, 6066–6069; j) Y. Zhang, D. Li, R. Clérac, M. Kalisz, C.

Mathonière, S. M. Holmes, *Angew. Chem. Int. Ed.* **2010**, *49*, 3752–3756; *Angew. Chem.* **2010**, *122*, 3840–3844.
[6] a) A. Mondal, Y. Li, P. Herson, M. Seuleiman, M.-L. Boillot, E. Rivière, M. Julve, L. Rechignat, A. Bousseksou, R. Lescouëzec, *Chem. Commun.* **2012**, *48*, 5653–5655; b) A. Mondal, Y. Li, L.-M. Chamoreau, M. Seuleiman, L. Rechignat, A. Bousseksou, M.-L. Boillot, R. Lescouëzec, *Chem. Commun.* **2014**, *50*, 2893–2895; c) S. De, J.-R. Jiménez, Y. Li, L.-M. Chamoreau, A. Flambard, Y. Journaux, A. Bousseksou, R. Lescouëzec, *RSC Adv.* **2016**, *6*, 17456–17459; d) Y. Li, A. Benchohra, B. Xu, B. Baptiste, K. Béneut, P. Parisiades, L. Delbes, A. Soyer, K. Boukheddaden, R. Lescouëzec, *Angew. Chem. Int. Ed.* **2020**, *59*, 17272–17276; *Angew. Chem.* **2020**, *132*, 17425–17429; e) Q. P. Xuan, J. Glatz, A. Benchohra, J.-R. Jiménez, R. Plamont, L.-M. Chamoreau, A. Flambard, Y. Li, L. Lisnard, D. Dambournet, O. J. Borkiewicz, M.-L. Boillot, L. Catala, A. Tissot, R. Lescouëzec, *J. Mater. Chem. C* **2021**, *9*, 8882–8890.
[7] a) D. Garnier, A. Mondal, Y. Li, P. Herson, L.-M. Chamoreau, L. Toupet, M. Buron Le Cointe, E. M. B. Moos, F. Breher, R. Lescouëzec, *C. R. Chim.* **2019**, *22*, 516–524; b) J. Glatz, L.-M. Chamoreau, A. Flambard, J.-F. Meunier, A. Bousseksou, R. Lescouëzec, *Chem. Commun.* **2020**, *56*, 10950–10953.
[8] a) T. M. Ozvat, A. K. Rappé, J. M. Zadrozny, *Inorg. Chem.* **2022**, *61*, 778–785; b) R. Bramley, M. Brorson, A. M. Sargeson, C. E. Schaeffer, *J. Am. Chem. Soc.* **1985**, *107*, 2780–2787.
[9] a) J. C. C. Chan, S. C. F. Au-Yeung in *Cobalt-59 NMR spectroscopy, Vol. 41* Academic Press, **2000**, pp. 1–54; b) C. W. Kirby, W. P. Power, *Can. J. Chem.* **2001**, *79*, 296–303; c) S. S. Massoud, *Polyhedron* **1994**, *13*, 3127–3134; d) A. Medek, L. Frydman, *J. Am. Chem. Soc.* **2000**, *122*, 684–691; e) A. Medek, V. Frydman, L. Frydman, *Proc. Nat. Acad. Sci.* **1997**, *94*, 14237–14242; f) A. Medek, V. Frydman, L. Frydman, *J. Phys. Chem. B* **1997**, *101*, 8959–8966; g) A. Medek, V. Frydman, L. Frydman, *J. Phys. Chem. A* **1999**, *103*, 4830–4835; h) W. P. Power, C. W. Kirby, N. J. Taylor, *J. Am. Chem. Soc.* **1998**, *120*, 9428–9434; i) M. P. J. Peeters, M. J. van Bommel, P. M. C. Neilen-ten Wolde, H. A. M. van Hal, W. C. Keur, A. P. M. Kentgens, *Solid State Ionics* **1998**, *112*, 41–52; j) R. Siegel, J. Hirschinger, D. Carlier, S. Matar, M. Ménétrier, C. Delmas, *J. Phys. Chem. B* **2001**, *105*, 4166–4174.
[10] a) M. Duffiet, M. Blangero, P. E. Cabelguen, K. S. Song, F. Fauth, C. Delmas, D. Carlier, *Inorg. Chem.* **2020**, *59*, 2890–2899; b) K. M. N. Burgess, C. M. Widdifield, Y. Xu, C. Leroy, D. L. Bryce, *ChemPhysChem* **2018**, *19*, 227–236; c) G. S. Reddy, M. Manjunatha, K. P. Ramesh, *J. Phys. Chem. Solids* **2021**, *148*, 109703; d) T. Pathmalingam, F. Habib, C. M. Widdifield, F. Loiseau, T. J. Burchell, S. I. Gorelsky, A. M. Beauchemin, D. L. Bryce, M. Murugesu, *Dalton Trans.* **2010**, *39*, 1504–1510.
[11] a) G. Aromí, A. S. Batsanov, P. Christian, M. Helliwell, A. Parkin, S. Parsons, A. A. Smith, G. A. Timco, R. E. P. Winpenny, *Chem. Eur. J.* **2003**, *9*, 5142–5161; b) A. B. Boeer, A.-L. Barra, L. F. Chibotaru, D. Collison, E. J. L. McInnes, R. A. Mole, G. G. Simeoni, G. A. Timco, L. Ungur, T. Unruh, R. E. P. Winpenny, *Angew. Chem. Int. Ed.* **2011**, *50*, 4007–4011; *Angew. Chem.* **2011**, *123*, 4093–4097.
[12] a) D. Casanova, M. Llunell, P. Alemany, S. Alvarez, *Chem. Eur. J.* **2005**, *11*, 1479–1494; b) M. C. Llunell, D. Cirera, J. Bifill, J–M. Alemany, P. Alvarez, S. Pinsky, M. Avnir in *SHAPE: Continuous shape measures of polygonal and polyhedral molecular fragments, Vol.* Universitat de Barcelona, Barcelona, Spain, Barcelona, **2005**.
[13] M.-G. Alexandru, D. Visinescu, N. Marino, G. De Munno, J. Vallejo, F. Lloret, M. Julve, *Eur. J. Inorg. Chem.* **2014**, *27*, 4564–4572.
[14] a) S. Chorazy, M. Rams, J. Wang, B. Sieklucka, S.-i. Ohkoshi, *Dalton Trans.* **2017**, *46*, 13668–13672; b) C.-H. Tan, X. Ma, Q.-L. Zhu, Y.-H. Huang, Y.-H. Wen, S.-M. Hu, T.-L. Sheng, X.-T. Wu, *CrystEngComm* **2012**, *14*, 8708–8713; c) R. C. Aggarwal, V. C. Sekhar, *Curr. Sci.* **1979**, *48*, 286–289.
[15] K.-Y. A. Lin, B.-J. Chen, C.-K. Chen, *RSC Adv.* **2016**, *6*, 92923–92933.
[16] a) K. Fukui, H. Ohya-Nishiguchi, N. Hirota, *Bull. Chem. Soc. Jpn.* **1991**, *64*, 1205–1212; b) J. M. Zadrozny, J. Liu, N. A. Piro, C. J. Chang, S. Hill, J. R. Long, *Chem. Commun.* **2012**, *48*, 3927–3929.
[17] D. Li, R. Clérac, O. Roubeau, E. Harté, C. Mathonière, R. Le Bris, S. M. Holmes, *J. Am. Chem. Soc.* **2008**, *130*, 252–258.
[18] R. J. Archer, C. S. Hawes, G. N. L. Jameson, V. McKee, B. Moubaraki, N. F. Chilton, K. S. Murray, W. Schmitt, P. E. Kruger, *Dalton Trans.* **2011**, *40*, 12368–12373.
[19] S. De, L.-M. Chamoreau, H. El Said, Y. Li, A. Flambard, M.-L. Boillot, S. Tewary, G. Rajaraman, R. Lescouëzec, *Front. Chem.* **2018**, *6*, 326.
[20] P. Gütlich, A. Hauser, *Coord. Chem. Rev.* **1990**, *97*, 1–22.
[21] S. De, S. Tewary, D. Garnier, Y. Li, G. Gontard, L. Lisnard, A. Flambard, F. Breher, M.-L. Boillot, G. Rajaraman, R. Lescouëzec, *Eur. J. Inorg. Chem.* **2018**, *3–4*(2), 414–428.
[22] K. Kaushik, S. Ghosh, S. Kamilya, M. Rouzières, S. Mehta, A. Mondal, *Inorg. Chem.* **2021**, *60*, 7545–7552.
[23] a) A. Flambard, F. H. Köhler, R. Lescouëzec, *Angew. Chem. Int. Ed.* **2009**, *48*, 1673–1676; *Angew. Chem.* **2009**, *121*, 1701–1704; b) A. Flambard, F. H. Köhler, R. Lescouëzec, B. Revel, *Chem. Eur. J.* **2011**, *17*, 11567–11575; c) A. Flambard, A. Sugahara, S. De, M. Okubo, A. Yamada, R. Lescouëzec, *Dalton Trans.* **2017**, *46*, 6159–6162.
[24] a) N. F. Ramsey, *Phys. Rev.* **1950**, *78*, 699–703; b) A. Yamasaki, *J. Coord. Chem.* **1991**, *24*, 211–260.
[25] a) J. S. Griffith, L. E. Orgel, *Trans. Faraday Soc.* **1957**, *53*, 601–606; b) N. Juranić, *Coord. Chem. Rev.* **1989**, *96*, 253–290.
[26] a) A. J. Pell, G. Pintacuda, C. P. Grey, *Prog. Nucl. Magn. Reson. Spectrosc.* **2019**, *111*, 1–271; b) Y. Zhang, H. Sun, E. Oldfield, *J. Am. Chem. Soc.* **2005**, *127*, 3652–3653.
[27] S. C. F. Au-Yeung, D. R. Eaton, *J. Magn. Reson.* **1983**, *52*, 351–365.
[28] Tyler M. Ozvat, M. E. Peña, J. M. Zadrozny, *Chem. Sci.* **2019**, *10*, 6727–6734.
[29] a) F. H. Köhler, R. Lescouëzec, *Angew. Chem. Int. Ed.* **2004**, *43*, 2571–2573; *Angew. Chem.* **2004**, *116*, 2625–2627; b) N. Baumgärtel, A. Flambard, F. H. Köhler, R. Lescouëzec, *Inorg. Chem.* **2013**, *52*, 12634–12644.

Manuscript received: March 11, 2022
Accepted manuscript online: June 18, 2022
Version of record online: July 20, 2022